Chinese Chemical Letters 35 (2024) 108343

Contents lists available at ScienceDirect

Chinese Chemical Letters

journal homepage: www.elsevier.com/locate/cclet

Self-adaptive hydrogel for breast cancer therapy *via* accurate tumor elimination and on-demand adipose tissue regeneration

Ran Tian[a,1], Xinyu Qiu[b,1], Wenyun Mu[a], Bolei Cai[c], Zhongning Liu[d], Shiyu Liu[e,*], Xin Chen[a,*]

[a] *School of Chemical Engineering and Technology, Department of Chemical Engineering, Shaanxi Key Laboratory of Energy Chemical Process Intensification, Xi'an Jiao Tong University, Xi'an 710049, China*
[b] *School of Stomatology, State Key Laboratory of Military Stomatology & National Clinical Research Center for Oral Diseases & Shaanxi Clinical Research Center for Oral Diseases, Department of Preventive Dentistry, The Fourth Military Medical University, Xi'an 710032, China*
[c] *School of Stomatology, State Key Laboratory of Military Stomatology, Department of Oral and Maxillofacial Surgery, The Fourth Military Medical University, Xi'an 710032, China*
[d] *Department of Prosthodontics, Peking University School and Hospital of Stomatology, National Clinical Research Center for Oral Diseases, National Engineering Laboratory for Digital and Material Technology of Stomatology, Beijing Key Laboratory of Digital Stomatology, Beijing 100081, China*
[e] *School of Stomatology, State Key Laboratory of Military Stomatology, National Clinical Research Center for Oral Diseases, Shaanxi International Joint Research Center for Oral Diseases, Center for Tissue Engineering, The Fourth Military Medical University, Xi'an 710032, China*

ARTICLE INFO

Article history:
Received 6 December 2022
Revised 7 March 2023
Accepted 14 March 2023
Available online 17 March 2023

Keywords:
Smart hydrogel with self-adaptable size
Breast cancer therapy
Dual responsive cargoes release
Selective tumor elimination
On-demand adipose tissue regeneration
Effective bacteria inhibition

ABSTRACT

The irregular defects and residual tumor tissue after surgery are challenges for effective breast cancer treatment. Herein, a smart hydrogel with self-adaptable size and dual responsive cargos release was fabricated to treat breast cancer *via* accurate tumor elimination, on-demand adipose tissue regeneration and effective infection inhibition. The hydrogel consisted of thiol groups ended polyethylene glycol (SH-PEG-SH) and doxorubicin encapsulated mesoporous silica nanocarriers (DOX@MSNs) double crosslinked hyaluronic acid (HA) after loading of antibacterial peptides (AP) and adipose-derived stem cells (ADSCs). A pH-cleavable unsaturated amide bond was pre-introduced between MSNs and HA frame to perform the tumor-specific acidic environment dependent DOX@MSNs release, meanwhile an esterase degradable glyceryl dimethacrylate cap was grafted on MSNs, which contributed to the selective chemotherapy in tumor cells with over-expressed esterase. The bond cleavage between MSNs and HA would also cause the swelling of the hydrogel, which not only provide sufficient space for the growth of ADSCs, but allows the hydrogel to fully fill the irregular defects generated by surgery and residual tumor atrophy, resulting in the on-demand regeneration of adipose tissue. Moreover, the sustained release of AP could be simultaneously triggered along with the size change of hydrogel, which further avoided bacterial infection to promote tissue regeneration.

Breast cancer is one of the most commonly cancer among women which has the second highest death rate [1]. Nowadays, using surgery to remove tumor tissue along with some surrounding healthy tissue is still the major approach for clinical treatment [2]. However, this strategy would cause serious tissue defects on breast, which breaks its natural shape, resulting in negative psychological effects such as anxiety, insomnia, depressive attitudes and even suicide in severe cases [3]. Moreover, the mastectomy cannot completely eliminate all the tumor cells, these residual tumor cells will proliferate over days and then lead to cancer recurrence [4].

As to prevent the possible tumor recurrence meanwhile to reconstruct the breast, systemic and local chemotherapy based on toxic anti-tumor drugs and photothermal therapy based on various photothermal agents were respectively combined with tissue engineering scaffolds for effective treatment to breast cancer [5–14]. This therapeutic strategy of loading stem cells into scaffolds can induce adipose stem cells to differentiate into adipose tissue and achieve the filling of defects after tumor surgery [15–17]. Although this strategy opened a window for the integration of tumor elimination and tissue regeneration to solve the sequel of surgery, the nonspecific toxic drugs or heating may cause serious random damages to the pre-seeded stem cells, even the normal

* Corresponding authors.
E-mail addresses: liushiyu@vip.163.com (S. Liu), chenx2015@xjtu.edu.cn (X. Chen).
[1] These authors contributed equally to this work.

https://doi.org/10.1016/j.cclet.2023.108343
1001-8417/

tissues surrounding tumor, which not only limited the tissue regeneration efficiency but results in endless suffering to patients [18–20]. Furthermore, current integrative scaffolds for tumor elimination and tissue engineering were all designed with fixed and regular shape [21–25]. This regular shape limited the application of current scaffolds for repairing irregular tissue defects caused by clinical surgery, which are varies from patient to patient [26]. More importantly, the scaffolds with fixed shape are impossible to fill the tissue gap generated by elimination of tumor tissue after chemotherapy or photothermal therapy, which may cause incomplete tissue regeneration and fibrous tissue overgrowth, resulting in a dysfunctional new tissue. In addition, current scaffolds are vulnerable to opportunistic microorganisms during implantation, leading to possible infection and inflammatory response *in vivo*, which is a serious threat for tissue engineering constructs [27–30]. Therefore, it is keen to develop a new scaffold which is able to 1) selectively damage residual breast tumor cells for accurate chemotherapy, 2) spontaneously change its shape for fully filling certain breast defect after surgical treatment and chemotherapy, 3) promote the growth of preloaded stem cells for generation of new tissue and 4) provide antimicrobial environment to avoid infection during implantation for effective tissue construction.

Recently, the tumor microenvironment (TME) has been exploited to assist with conventional strategies to achieve an effective and tumor-specific therapy, owing to the TME is prominently different as normal tissues [31–34]. Therefore, using the multiple TME to trigger the accurate delivery of anti-tumor drugs from scaffold to tumor cells, to spatiotemporally manipulate the shape of scaffold as required, meanwhile to induce the release of antimicrobial agents, may offer a solution to solve the above issues. Herein, we fabricated a pH and esterase dual responsive nano-composite hydrogel scaffold *via* click chemistry and coordinate chemistry, in which the methacrylic anhydride grafted hyaluronic acid (C=C–HA) was used as frame, the thiol groups ended polyethylene glycol (SH-PEG-SH) and carboxyl modified mesporous silica nanocarriers (MSN–COOH) assisted by ferric ions were used as cross-linkers, respectively. The MSNs were pre-filled by DOX and poly glyceryl dimethacrylate (MSN@DOX-PGD), which was also designed an unsaturated amide bond on its surface between silica and carboxyl. After loading antibacterial peptides (AP) and adipose-derived stem cells (ADSCs), this hydrogel (HA-MSN@DOX-AP-AD) was expected to perform accurate tumor elimination, on-demand adipose tissue regeneration and inhibition of bacterial infection for effective breast cancer treatment (Scheme 1a).

Before therapy, the short coordinate bond between MSN@DOX-PGD and HA maintained a compact structure of the hydrogel, which limited the leakage of the MSN@DOX-PGD and pre-loaded antibacterial peptides from the hydrogel. Once the hydrogel was implanted to the tumor area, the acid tumor microenvironment would cleave the unsaturated amide bonds [35], resulting in a gradual swell accompanying with the release of antibacterial peptides and MSN@DOX-PGD. The detached MSN@DOX-PGD would further enter tumor cells through endocytosis, and then the PGD cap would be degraded by abundant esterase in tumor cells to release DOX for intracellular chemotherapy [36], leading to negligible side effect to the pre-seeded adipose-derived stem cells and surrounding healthy cells. The swelled hydrogel would completely fill the original defects caused by surgery and new defects generated by tumor elimination after chemotherapy, which provides an extracellular matrix (ECM)-mimicking environment with porous architecture to promote the proliferation and differentiation of adipose-derived stem cells, facilitating on-demand tissue regeneration. Moreover, the released antibacterial peptides would simultaneously damage the bacteria introduced by hydrogel implantation to avoid the infection and inflammation, which may impede the tissue regeneration (Scheme 1b).

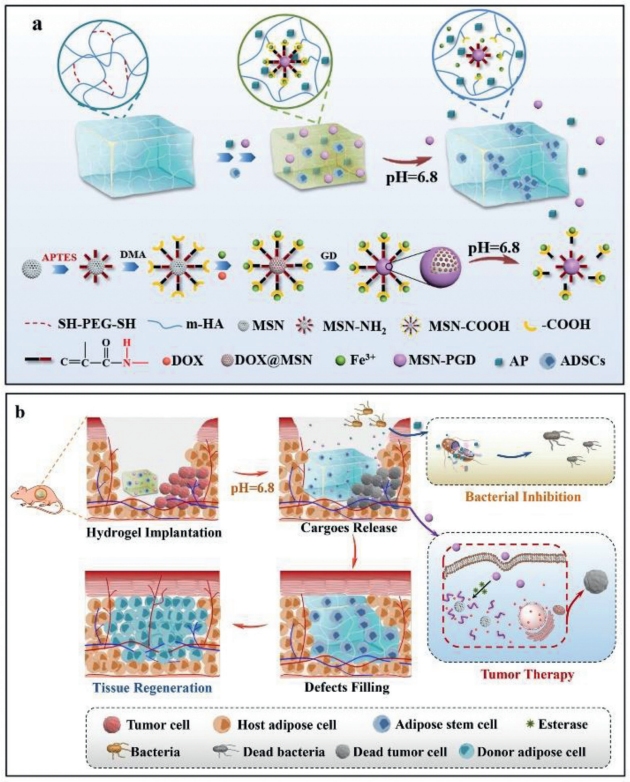

Scheme 1. Schematic illustration of fabrication (a) and therapeutic process (b) of the pH/enzyme dual responsive ADSCs-loaded HA-MSN@DOX-AP hydrogel, which was expected to combine tumor selective chemotherapy, on-demand antibacterial property and controllable adipose tissue regeneration for effective breast cancer treatment.

To prepare the hydrogel, methacrylic anhydride grafted hyaluronic acid (C=C–HA) was synthesized *via* nucleophilic reaction between hydroxyl group and methacrylic anhydride (MA) (Scheme S1 in Supporting information). The modification process was verified by nuclear magnetic resonance spectroscopy (^{1}H NMR, Fig. 1a) and infrared spectroscopy (IR, Fig. S1 in Supporting information), which presented obvious characteristic proton signals of MA (H connected with unsaturated double bond) and typical vibration peak of the unsaturated double bond, indicating the successful generation of the C=C–HA. After that, the MSNs with pore size about 3–4 nm (Fig. S2 in Supporting information) were synthesized and grafted by amino groups through the method previously reported by our group [36]. The resulting MSN–NH_2 further reacted with 2,3-dimethylmaleic anhydride (DMA) to introduce carboxyl groups on MSNs with pH cleavable unsaturated amide bonds in between, which was named as MSN–COOH (Scheme S2 in Supporting information). The sequential fabrication of MSNs was investigated by Fourier transform infrared (FTIR) spectrometry and zeta potential measurement, which clearly showed characteristic vibrations of NH_2 and COOH (FTIR, Fig. 1b) as well as the corresponding change of surface charges (zeta potential, Fig. 1c).

Transmission electron microscopy (TEM) was employed to provide more information about the MSN–COOH (Fig. 1d). The TEM results showed that our MSN–COOH is about 200 nm in diameter with spherical shape and obvious large pores. The pores on MSN–COOH was used to load doxorubicin (DOX) and glyceryl dimethacrylate followed with *in situ* polymerization of glyceryl dimethacrylate to block the pores (Scheme S3 in Supporting information), which not only avoid the premature release of DOX before arriving designed location, but provide stimuli-

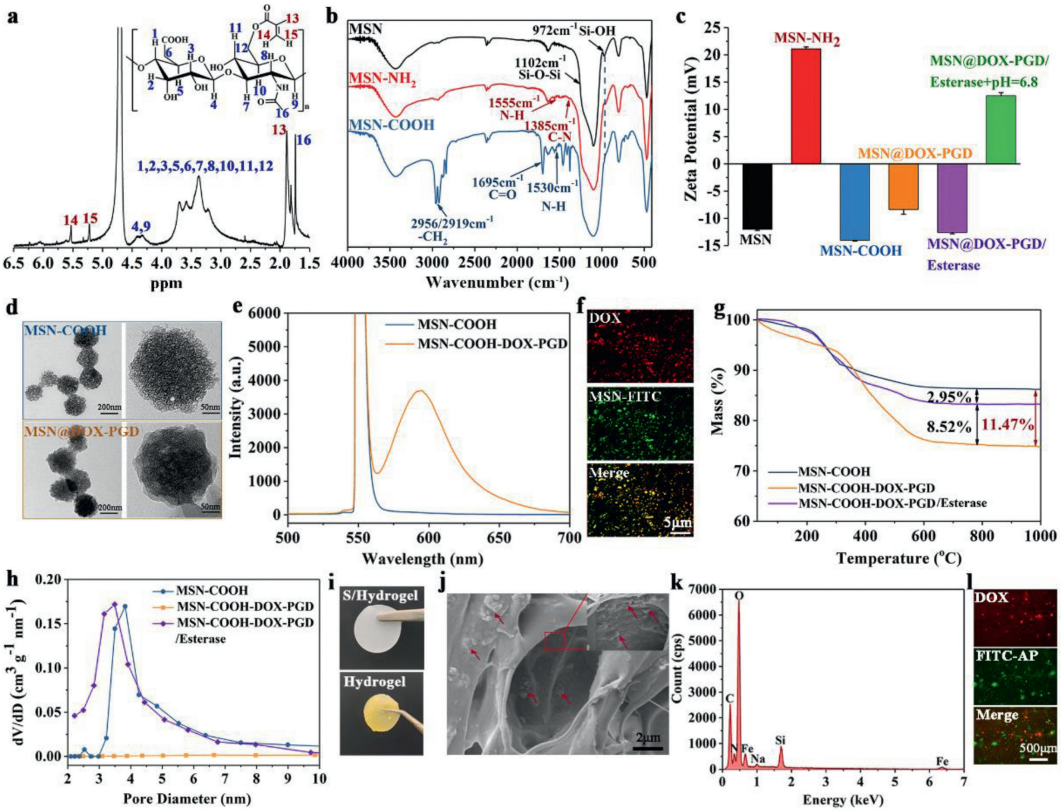

Fig. 1. (a) ^{1}H NMR of methacrylic anhydride modified hyaluronic acid (C=C–HA). (b) IR spectrometry of MSNs before and after each step of functionalization, which presented certain characteristic peaks corresponding to designed chemical structures. (c) Zeta-potential of MSNs before and after each step of functionalization, which presented certain surface charges corresponding to designed chemical structures. The surface charge of MSN@DOX-PGD at pH 6.8 and esterase was also presented in this picture, which switched back to positive charge similar with MSN–NH_2, indicating the appearance of pH cleavable bonds between MSN and functional groups. (d) The TEM images of MSN–COOH before and after DOX/polyester loading. (e) The fluorescence spectrum of MSN–COOH before and after DOX/polyester loading. (f) The fluorescence microscope images of the MSN@DOX-PGD where the MSNs were pre-labeled by FITC. These images directly showed the successful loading of DOX. (g) The TGA of MSN–COOH, MSN@DOX-PGD and MSN@DOX-PGD after esterase treatment. (h) The pore-size distribution of MSN–COOH, MSN@DOX-PGD and MSN@DOX-PGD after esterase treatment, indicating that the DOX could be encapsulated in the porous structure of MSNs and completely capped by polyester, which could be released after the polyester degradation included by esterase. (i) The photograph of the single crosslinked hydrogel (S/Hydrogel) and HA-MSN@DOX-AP hydrogel. (j) The SEM images of HA-MSN@DOX-AP hydrogel. The red arrows pointed the locations of MSN@DOX-PGD. (k) The EDS of HA-MSN@DOX-AP hydrogel, which shows obvious signal of silicon and iron, indicating the existence of Fe^{3+} as the bridge ion to connect MSNs and HA in the hydrogel. (l) The fluorescence microscope images of the HA-MSN@DOX-AP hydrogel where the AP was pre-labeled by FITC. These images directly showed the successful co-loading of both DOX and AP in this hydrogel.

responsive drug release triggered by the overexpressed esterase in tumor cells due to the enzymatic hydrolysis of ester bonds [37], resulting in the tumor specific chemotherapy. The MSNs after DOX loading and polyester capping (MSN@DOX-PGD) was also investigated by TEM, which presented complete blockage of the pores after *in situ* polymerization (Fig. 1d). The particle size of MSN–COOH and MSN@DOX-PGD were also recorded by dynamic light scattering (Fig. S3), which presented increasing size from 200 nm of MSN–COOH to 220 nm after polymerization. The resulting MSN@DOX-PGD was further investigated by fluorescence spectrum, which performed strong characteristic fluorescence of DOX at 600 nm (Fig. 1e). The signal of DOX is exactly matching the signal of MSNs [fluorescein isothiocyanate (FITC) labelled MSNs] in the images of fluorescence microscope (Fig. 1f), providing direct evidence of the successful encapsulation of DOX in the pores of MSNs. Moreover, the calculated cargo encapsulation efficiency of MSNs at different DOX/MSN weight ratios are listed in Table S1 (Supporting information). The encapsulation efficiency of DOX on MSNs@DOX-PGD reached 82%, which demonstrated the excellent loading capacity of MSNs. As expected, the PGD cap could be effectively degraded once the MSN@DOX-PGD was incubated in the solution containing esterase, which simultaneously caused the escape of DOX, resulting in the significant mass loss (Fig. 1g), the re-appearance of pores on MSN@DOX-PGD similar with that on MSN–COOH (Fig. 1h), and the clear charge recover close to MSN–COOH (Fig. 1c). Moreover, the additional incubation of esterase treated MSN@DOX-PGD in phosphate buffered solution (PBS) at pH 6.8 further turned its surface change from negative to positive, which is similar with the surface change of MSN–NH_2, indicating the pH triggered cleavage of the unsaturated amide bond as design (Fig. 1c).

The as-synthesized MSN@DOX-PGD was further mixed with C=C–HA, Fe^{3+}, antibacterial peptides and commercially available SH-PEG-SH to prepare hydrogel, where the click reaction between SH-PEG-SH and C=C groups on HA under ultraviolet (UV) irradiation as well as the coordination interaction between Fe^{3+} and COOH groups on both HA and MSNs were used to crosslink this hydrogel (Scheme S4 in Supporting information). The photographs of hydrogels before and after crosslinked by MSN–COOH was shown in Fig. 1i. Moreover, the morphology of the resulting HA-MSN@DOX-AP hydrogel was investigated by scanning electron microscope (SEM, Fig. 1j). As can be seen from this figure, the hydrogel has a porous structure with 10 μm in diameter, which contained plenty of MSNs on the wall of these pores. The well-maintained porous structure (essential for cell-seeding and mass transport) even after loading of the MSN@DOX-PGD and antibacterial peptides indicated the potential of this complex hydrogel for tissue regeneration. The chemical component of this hydrogel was obtained by energy dispersive X-ray spectroscopy (EDS), which shows obvious signal of silicon and iron, indicating the ex-

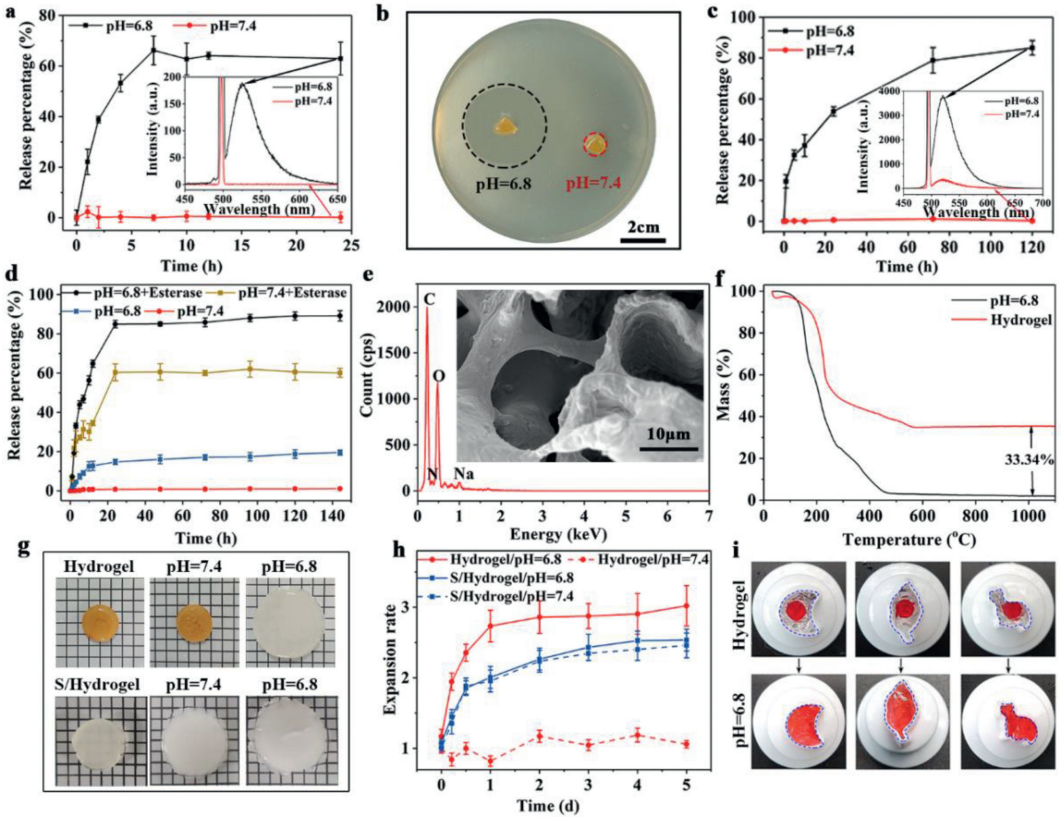

Fig. 2. (a) The pH-dependent release kinetics of AP from the HA-MSN@DOX-AP hydrogel. (b) Digital photographs of bacteriostatic ring of HA-MSN@DOX-AP hydrogel against *S. aureus* after treatment by PBS with pH 7.4 or pH 6.8. (c) The pH-dependent release kinetics of MSN@DOX-PGD from the HA-MSN@DOX-AP hydrogel. (d) The pH/enzyme-dependent release kinetics of DOX from MSNs. (e) The SEM images and EDS of HA-MSN@DOX-AP hydrogel after treatment by PBS with pH 6.8, which shows neither MSNs or signal of silicon, indicating the complete release of MSN@DOX-PGD. (f) The TGA of the HA-MSN@DOX-AP hydrogel before and after treatment by PBS with pH 6.8, indicating the exact amount of MSN@DOX-PGD in the hydrogel, which could fully escape from the hydrogel under proper stimulation. (g) The photograph of HA-MSN@DOX-AP hydrogel and the single crosslinked hydrogel before and after treatment by PBS with pH 7.4 and pH 6.8. (h) The pH triggered volume change of HA-MSN@DOX-AP hydrogel and the single crosslinked hydrogel before and after treatment by PBS with pH 7.4 and pH 6.8. (i) Self-adaption of the HA-MSN@DOX-AP hydrogel under tumor-specific acid environment.

istence of Fe^{3+} and MSN@DOX-PGD, where the Fe^{3+} served as the bridge ion to connect MSNs and HA in the hydrogel (Fig. 1k). The co-encapsulation of MSN@DOX-PGD and AP in the resulting hydrogel (HA-MSN@DOX-AP) were further demonstrated by fluorescence microscope (Fig. 1l), where the antibacterial peptides were pre-labeled by FITC. As can be seen from this figure, obvious red fluorescence (from DOX in MSNs) and green fluorescence (from FITC-AP) simultaneously appeared in the hydrogel, indicating the successful formation of the HA-MSN@DOX-AP hydrogel.

The pH and enzyme triggered triple release (i: antibacterial peptides escaped from the hydrogel, ii: MSN@DOX-PGD detached from hydrogel and iii: DOX released form MSNs) was investigated under simulated physiological conditions of body fluid (pH 7.4), extracellular matrix of tumor (pH 6.8) and the lysosome of tumor (pH 6.8 with rich of esterase). The amounts of antibacterial peptides and MSN@DOX-PGD detached from the hydrogel were separately determined by monitoring the fluorescence intensity at 530 nm (characteristic emission peak of fluorescein isothiocyanate) as a function of time using fluorescence spectrum, where either antibacterial peptides or MSNs were pre-labeled by FITC. As can be seen from Fig. 2a, the release profiles of antibacterial peptides from the hydrogel is highly pH dependent. At pH 7.4, less than 5% of antibacterial peptides appeared in the solution even after 24 h incubation. However, the release rate of the antibacterial peptides at pH 6.8 dramatically increased comparing with that at pH 7.4, and the release percentage reach about 70% only after 7 h incubation. The released antibacterial peptides presented great antimicrobial effect, which generated a large bacteriostatic growth ring with diameter about 3.41 cm (Fig. 2b). In contrast, the hydrogel at pH 7.4 did not show visible bacteria inhibition. All these results indicated that the antimicrobial process would start in the acid environment of tumor tissue along with the tumor therapy and tissue regeneration as expected.

Much slow release with similar pH responsiveness as antibacterial peptides was observed on FITC-labeled MSNs (Fig. 2c). The MSNs could be fully encapsulated in the hydrogel with less than 5% of leakage up to 120 h incubation in PBS at pH 7.4, while the incubation in PBS at pH 6.8 with same time period would cause over 80% of MSNs release. The enzyme triggered DOX release from MSNs was further determined by monitoring the fluorescence intensity at 600 nm (characteristic emission peak of DOX) as a function of time using same fluorescence spectrum. It can be observed from Fig. 2d that only less than 20% of DOX release could be observed from MSNs in its "closed" stage even after 140 h of incubation in PBS regardless of the pH value. However, the DOX release immediately appeared after adding esterase, due to the enzymatic degradation of the PGD cap, which was completed in 20 h with the final release percentage being over 85%.

Moreover, the release procedure of MSN@DOX-PGD could be directly observed from SEM images and EDS. As can be seen from Fig. 2e, large holes with smooth wall appeared in the hydrogel, where no MSNs and silicon signal could be detected, indicating the complete detachment of MSN@DOX-PGD under acid condition (simulated environment of tumor tissue). To quantify this procedure, the thermos gravimetric analysis (TGA) of the complex hydrogel before and after incubation in acid environment

were performed (Fig. 2f), which shows about 33% of mass difference, indicating that each gram of hydrogel could provide up to 330 mg of DOX loaded MSNs in tumor environment for further therapy.

The responsiveness to tumor environment (low pH value) could be attributed to the cleavage of unsaturated amide bonds between the MSNs and HA framework, which not only caused the visible 3 times swelling of the hydrogel on the macroscopic level to fully fill the irregular defects after tumor therapy (Figs. 2g and h), but also resulted obvious enlargement of the proses for better cell growth of ADSC to regenerate adipose tissue with required size (Fig. 2e). In contrast, single crosslinked hydrogel showed mild swelling at both different pH due to the swelling properties, which unable to perform selective release of the drug. To further demonstrate the on-demand self-adaptability of the HA-MSN@DOX-AP hydrogel after pH triggered swelling, the hydrogels (dyed with red ink) were placed in much larger containers with different shapes. As can be seen from Fig. 2i, the hydrogel could completely fill the container and exactly match its shape after soaking in PBS with pH 6.8 for 24 h, which was expected to fit the irregular defects caused during tumor therapy for better tissue regeneration.

The cleavage of the unsaturated amide bonds in hydrogel after incubation in acid environment was further verified by its mechanical property change, which shows obvious decrease of the G' and G" to the level of hydrogel only crosslinked by SH-PEG-SH, indicting the complete break of the unsaturated amide bonds under low pH (Fig. S4 in Supporting information). All these results well exhibited the stepwise activities of our hydrogel combining multiple stimuli responsive two-step delivery of DOX for highly selective chemotherapy to tumor cells and on-demand structure change of the hydrogel for formation of proper adipose tissue with requested shape and size, which could be used for effective treatment of breast cancer after surgery.

To explore the *in vitro* tumor therapeutic capacity of HA-MSN@DOX-AP hydrogel, the selective delivery of DOX to tumor cells were qualitatively and quantitatively investigated by confocal fluorescence microscopy (Fig. S5a in Supporting information) and flow cytometry (Figs. S5b and c in Supporting information) after co-incubating the hydrogel with MCF-10a cells at pH 7.4 (representative normal control) and with MCF-7 cells at pH 6.8 (representative breast cancer), respectively. As shown in Fig. S5a, some red fluorescence (DOX) was accumulated in the nucleus of MCF-7 cells only after 4 h co-culture, due to the DOX's mechanism of action as a DNA intercalating agent [38]. This fluorescence intensity dramatically enhanced against time, which shows strong bright-red color at 24 h, indicating the effective delivery of DOX to tumor cells. The high uptake by tumor cells could be attributed the assistance of AP to open cell membrane [39], which was designed to release from the hydrogel prior to DOX in tumor environment (Fig. 2a and Fig. S5a). Moreover, since the DOX loaded in MSNs could not enter the nucleus owing to its mismatch with the nucleopore size [40], the appearance of DOX in the nucleus of MCF-7 cells also indicated the intracellular release of DOX from MSNs, which has been verified to be triggered by esterase in above results. In contrast, no visible red fluorescence could be observed in MCF-10a cells even after 24 h co-incubation, which demonstrated the high selectivity of our hydrogel specifically for tumor therapy. Flow cytometry was further employed to quantify the efficiency and selectivity of DOX delivery to tumor (MCF-7) cells and normal (MCF-10a) cells. As shown in the Figs. S5b and c, 86.5% of the MCF-7 cells showed remarkable intracellular accumulation of DOX after 24 h co-incubation. While only 7.94% of the MCF-10a cells were DOX positive after same co-incubation time. All these results exhibited that HA-MSN@DOX-AP hydrogel performed specific tumor responsiveness and selective transportation of DOX into tumor cells instead of healthy cells, resulting in a great candidate for accurate tumor chemotherapy.

To directly evaluate the tumor therapeutic effect, *in vitro* cytotoxicity of HA-MSN@DOX-AP hydrogel were tested on MCF-7 cells (pH 6.8) and MCF-10a cells (pH 7.4) by using Cell Counting Kit 8 assay (CCK-8, Dojindo Co., Ltd., Japan), where different incubation times were assessed. The HA-MSN hydrogel, HA-MSN-AP hydrogel and HA-MSN@DOX hydrogel were used as negative controls. As shown in Fig. S6a and b (Supporting information), the pure HA-MSN hydrogel without DOX and AP loading showed no toxicity to both MCF-7 cells and MCF-10a cells even after 48 h incubation, while the rest groups all showed highly selective cytotoxicity to tumor (MCF-7) cells only with the difference of efficiency. The HA-MSN-AP group showed relatively weak cytotoxicity to MCF-7 cells with the decrease of cell viability from about 100% to 75% (24 h incubation) and 65% (48 h incubation), respectively. Much stronger cytotoxicity to MCF-7 cells appeared in the group of HA-MSN@DOX hydrogel, which shows 55% cell viability after 24 h co-incubation, and the number further dropped to less than 35% after 48 h. The lowest cell viability of MCF-7 cells was observed after treatment by HA-MSN@DOX-AP hydrogel due to the enhanced penetration of DOX loaded MSNs through cell membrane assisted by AP, which performed only 15% of the cells surviving at 48 h. Quantitatively, the cytotoxicity of HA-MSN@DOX-AP hydrogel to MCF-7 cells, as determined from the cell viability, was three times and seven times higher than that to MCF-10a cells after 24 h and 48 h incubation, respectively. This high selectivity could be attributed to the acidity triggered escape of both DOX loaded MSNs and antibacterial peptides from hydrogel, as well as the subsequent esterase induced DOX release form MSN, which led to effective and accurate internalization of DOX in and only in tumor cells, resulting in high toxicity with negligible side effects to healthy cells.

Since the above results have demonstrated that the HA-MSN@DOX-AP hydrogel is promising for selective and effective tumor elimination at the cellular level, the *in vivo* therapy was performed by implanting the hydrogel beneath the tumor of the tumor-bearing nude mice. All experimental protocols were approved by the Animal Center of Fourth Military Medical University. The animal protocols were approved by the Animal Ethical and Care Committee of the Fourth Military Medical University. As can be seen from Fig. S7a (Supporting information), obvious swelling of the HA-MSN@DOX-AP hydrogel was observed at 24 h after implantation, indicating the release of MSN@DOX and antibacterial peptide were rapidly triggered in the acid environment around tumor tissue as design. The average tumor size after treatment were monitored for 2 weeks to further evacuate the therapeutic efficiency. The PBS and hydrogel without DOX or AP loading were used as negative controls. As shown in Fig. S7b (Supporting information), PBS treatment group showed the fastest tumor growth rate. While function groups (hydrogel containing either DOX or AP) presents obvious inhibition effect on tumor growth with different efficiency, due to the diverse chemotherapies based on tumor environment triggered DOX or AP release from the hydrogel. The strongest tumor inhibition was observed in the group of HA-MSN@DOX-AP hydrogel with synergistic effect of DOX and AP, where no obvious tumor growth appeared in 2 weeks. The pure hydrogel without DOX and AP loading was also investigated, which showed no tumor inhibition effect similar to the PBS group, indicating the antitumor property was mainly derived by AP and DOX assisted chemotherapy. To further assess the therapeutic efficacy, histological analysis using hematoxylin and eosin (H&E) staining was performed (Fig. S7c in Supporting information). Compared with the control groups (PBS group and hydrogel without DOX/AP), the tumors in the treatment groups showed different degrees of cell remission and apoptosis areas, among which tumors treated with HA-MSN@DOX-AP hydrogel showed the largest area of cell degeneration and tumor tissue disintegrating (red area), confirming its high efficiency in suppressing tumor growth.

As an important parameter for evaluating the therapeutic efficiency, the survival rates of mice receiving different treatments were also investigated (Fig. S8a in Supporting information). As can be seen from this figure, mice treated by PBS and pure hydrogel without DOX/AP did not survive over 42 and 44 days, respectively. Survival rate enhancement of these tumor-bearing mice appeared after treatment by hydrogel containing AP or DOX, which all ended with 30% in 2 months. Significantly, 84% mice treated with HA-MSN@DOX-AP hydrogel survived over 50 days. The high survival rate could be attributed to the tumor-specific chemotherapy *via* the synergistic effect of DOX and AP, which only damaged tumor tissue meanwhile generated neither weight loss of the mice nor pathological abnormalities in the major organs (heart, liver, spleen, lung and kidney) even to the end of the treatment (Figs. S8b and c in Supporting information), resulting in the negligible side-effects of healthy tissue during the tumor therapy based on our hydrogel. These evidences strongly suggested that the HA-MSN@DOX-AP hydrogel could potentially serve as a therapeutic platform for effective and accurate cancer treatment.

As we all known, bacterial infection during implantation may cause sustained and severe inflammatory response *in vivo*, which are detrimental to tissue regeneration. Thus, the antimicrobial property of the HA-MSN@DOX-AP hydrogel was assessed on *Escherichia coli* (*E. coli*, Gram-negative) and *Staphylococcus aureus* (*S. aureus*, Gram-positive) before using it to reconstruct the adipose tissue. Figs. S9a and b (Supporting information) showed that the hydrogel performed remarkable antimicrobial property against both *E. coli* and *S. aureus* under simulated tumor environment (pH 6.8) due to the acid triggered AP release, where the antibacterial ratio could reach up to 97.44% to *E. coli* and 99.99% to *S. aureus* after single time treatment.

The *in vivo* experiment was performed on mice after making the wound healing model and daubing with 100 μL of *S. aureus* [10^9 colony-forming units (cfu)] to further evaluate the ability of the HA-MSN@DOX-AP hydrogel, which was expected to present high antimicrobial activity to inhibit infection and inflammation. All mice were purchased from the Animal Center of Fourth Military Medical University. Beside the mouse treated by the HA-MSN@DOX-AP hydrogel, the mouse treated by pure hydrogel without AP/DOX loading and untreated mouse were chosen as negative controls. After that the skin samples from the infected wounds with different treatments were collected on day 3 and day 7, and the number of bacteria were counted after 24 h culture to investigate the antimicrobial activity of the HA-MSN@DOX-AP hydrogel *in vivo*. As shown in Figs. S10a–c (Supporting information), the samples without hydrogel treatment have a high content of bacteria with a number of 6.146 log cfu on day 3 and 6.079 log cfu on day 7. However, much lower numbers of 2.146 log cfu and 1.580 log cfu after 3- and 7-day treatment was observed for the pure hydrogel-treated group. It could be attributed to the Fenton reaction in bacteria induced by iron in the hydrogel, which is able to produce toxic reactive oxygen species (ROS) [9]. Moreover, the AP loading could further enhance the antibacterial efficacy of the hydrogel due to the synergistic effect, which performed the lowest bacterial survival rate *in vivo* (0.176 log cfu) with final log reduction of 5.779 against *S. aureus* after 7 days treatment.

Considering the continuous inflammation caused by bacterial infection is one of the critical issues impeding tissue regeneration, we further focus our study on inflammation control after verifying the anti-bacterial function of HA-MSN@DOX-AP hydrogel. It can be seen from Figs. S11a and b (Supporting information) that the inflammatory cells were significantly reduced after 7 days in both the pure hydrogel group and the HA-MSN@DOX-AP hydrogel group, where the latter is much more effective than the former, indicating the great ability of HA-MSN@DOX-AP hydrogel to control inflammation. Through the detection and analysis of the levels of pro-inflammatory factors, we found that the proinflammation-related genes [tumor necrosis factor-α (TNF-α), interleukin-6 (IL-6)] were significantly down-regulated by application of hydrogels, which indicated that the inflammation has been effectively and consistently suppressed. Moreover, we obviously found that the nascence and epithelization of some skin appendages structures, such as hair follicles, were completed partly in HA-MSN@DOX-AP hydrogel group at high magnification of Fig. S11a, indicating the effective inhibition of infectious inflammation provides conditions and foundations for creating a suitable immune microenvironment for tissue regeneration. All these results revealed that our hydrogel could achieve the sustained release of antibacterial peptide to eliminate surrounding bacteria, which is a promising candidate for applications of tissue regeneration while avoiding infection.

The adipose regeneration ability of HA-MSN@DOX-AP hydrogel after seeding human ADSCs was further evaluated by subcutaneous embedding model, where part of the hydrogel samples was pre-treated by PBS with pH 6.8 to simulate the tumor environment. Firstly, adhesion and growth of ADSCs in hydrogel was directly observed by confocal laser scanning microscope (Fig. S12 in Supporting information). It was noted that ADSCs grow well in the hydrogel with a large number of cells attached on the surface after 3 days incubation no matter with or without acid treatment. Then, the hydrogels containing human ADSCs were embedded subcutaneously in nude mice for 2 days. Further cellular information of culture was given by Terminal deoxynucleotidyl transferase dUTP nick-end labeling (TUNEL) assay. As can be seen from Figs. S13a and b (Supporting information), the dead cell content of hydrogel after acid treatment is significantly fewer than that of untreated hydrogel group, indicating a better environment for cell growth of the former group, due to its relatively large pore size after swelling.

To further investigate the adipogenesis efficiency of the hydrogel *in vivo*, subcutaneous embedding model was used. All nude mice were purchased from the Animal Center of Fourth Military Medical University. As shown in Figs. S14a and b (Supporting information), both hydrogels with or without acid treatment could form adipose tissue after 2 months of implantation, while the hydrogel pre-treated by PBS with pH 6.8 could form larger and heavier adipose tissue than the untreated hydrogel group. The histology staining showed plenty of new adipose cells in these generated tissues, which directly indicated the formation of adipose tissue (Fig. S15a in Supporting information). More information of these tissues was provided by histomorphometry measurement, which showed much more adipose tissue area newly formed on hydrogel after acid treatment than that on untreated hydrogel, indicating good accordance with our expectation (Fig. S15b in Supporting information). All these results indicated that the HA-MSN@DOX-AP hydrogel could significantly support the adhesion of ADSCs and stimulate adipogenesis *in vivo*. Moreover, to examine the *in vivo* degradation capacity of the hydrogel, a round HA-MSN@DOX-AP hydrogel with a diameter of 1.0 cm was divided into four equal parts, and then implanted in the subcutaneous ventral side of mice. After 28 days, the hydrogel could hardly be observed in Fig. S16 (Supporting information), proving the hydrogel was completely degraded. Meanwhile, this hydrogel is able to form adipose tissue with adjustable size according to the request, which could be a promising candidate to regenerate adipose tissue to completely fill the original and new defects caused by tumor surgery and further therapy, resulting in an effective approach for breast cancer therapy.

To evaluate the ability of HA-MSN@DOX-AP hydrogel after ADSCs seeding for integrative breast cancer treatment combining tumor elimination, infectious inhibition and adipose regeneration, we used a subcutaneous implantation model of *Staphylococcus aureus*-infected tumor-bearing mice (Fig. 3a). The PBS treated mice were

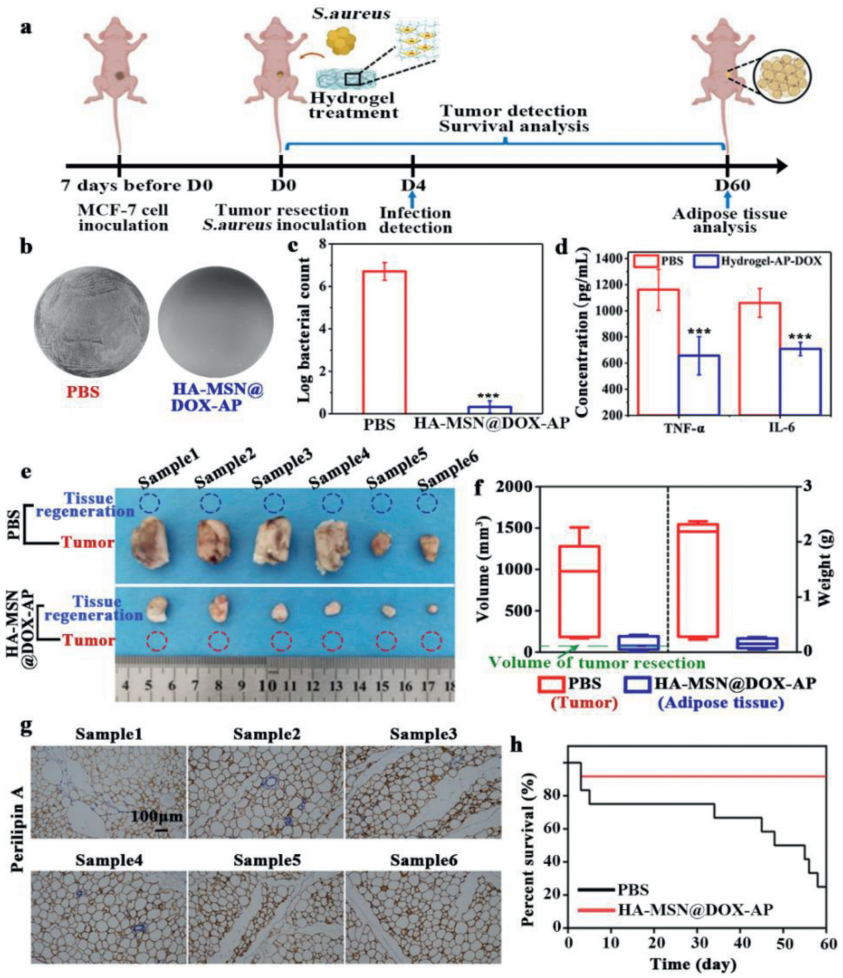

Fig. 3. (a) The schematic graph shows the protocol of model establishment for integrative breast cancer treatment by HA-MSN@DOX-AP hydrogel with ADSCs seeding *via* tumor elimination, infectious inhibition and adipose regeneration. (b, c) *In vivo* antibacterial activity of the ADSCs seeded HA-MSN@DOX-AP hydrogel, presenting by log reduction of *S. aureus* as well as the photographs of these bacteria from skin tissue after 4 days treatment by PBS and HA-MSN@DOX-AP hydrogel. (d) The concentration of immune factors in the skin tissue detected by ELISA kit at 4 days after therapy to measure the level of inflammation in PBS or hydrogel-AP-DOX treated groups. (e) The morphology photographs of the tissues from the original tumor site in PBS group and HA-MSN@DOX-AP hydrogel group after 2 months *in vivo* treatment. (f) The volume and weight of obtained tissues from the original tumor site (tumor tissue in PBS treated group and regenerated adipose tissue in HA-MSN@DOX-AP hydrogel treated group). (g) The immunohistochemical staining of the perilipin A in the regenerated adipose tissue. The scale bar represents 100 μm. (h) Survival curves of tumor-bearing and bacterial infected mice after the treatment of HA-MSN@DOX-AP and PBS. The data were collected with $n = 6$ per group, which are shown as mean ± standard deviation (SD), $^{***}P < 0.01$ *vs.* PBS treatment group.

used as the negative control group. The anti-bacterial property of the HA-MSN@DOX-AP hydrogel *in vivo* was first assessed. As to perform the experiment, the skin samples from the infected wounds with different treatments were collected at day 4 after implantation, and the number of bacteria in these skin samples were counted after 12 h of culture. Figs. 3b and c showed that the bacteria levels dropped from 6.7 log cfu to 0.3 log cfu in 4 days, indicating the great performance of our HA-MSN@DOX-AP hydrogel to inhibit the bacterial infection. The effective damage of bacteria further reduced the inflammation caused by infection, resulting in much lower levels of pro-inflammatory cytokines (TNF-α and IL-6) compared with the PBS-treated group (Fig. 3d).

As to demonstrate the hydrogel's property of tumor elimination and adipose regeneration, the subcutaneous tissue was removed after 2 months, which were illustrated in Fig. 3e. To further distinguish the type of tissue, histological analysis of H&E staining was performed in Fig. S17 (Supporting information). As can be seen from this figure, typical tumor tissue existed in PBS group, while the tumor disappeared and completely replaced by obvious adipose tissue in HA-MSN@DOX-AP hydrogel treated group. The average weight and volume of tumor and adipose were also statistically calculated, which showed that the regenerated adipose has similar volume as the original tumor, indicting the capacity of HA-MSN@DOX-AP hydrogel to perform both effective tumor elimination and on-demand repair of defects caused by tumor atrophy as design (Fig. 3f). The immunohistochemical staining of the regenerated adipose was further performed to identify whether this adipose tissue was derived from exogenous implanted adipose stem cells. As showed in Fig. 3g, the adipose tissue showed positive expression of human perilipin A, which demonstrated the adipose tissue was derived from implanted adipose stem cells rather than the mouse's own fat tissue. The replacement of tumor by adipose tissue also caused the significant enhancement of the survival rates of tumor-bearing mice. As showed in Fig. 3h, 90% of mice treated by HA-MSN@DOX-AP hydrogel survived over two months. In contrast, over 75% of mice died in the PBS group.

In summary, we have successfully prepared a pH and enzyme dual responsive hydrogel containing ADSCs, DOX loaded MSNs and AP for effective breast cancer therapy. During therapy, the two specific environments around tumor tissue (low pH value at 6.8) and in tumor cells (high content of esterase) would respectively trigger the release of DOX loaded MSNs from the hydrogel and DOX es-

cape from MSNs, resulting in a highly selective drug delivery into tumor for accurate tumor inhibition with negligible side effects to the seeded stem cells and surrounding healthy tissue. Meanwhile the pre-seeded adipose stem cells grow well in the hydrogel, which rapidly proliferate into adipose cells to regenerate new adipose tissue in several days even during the chemotherapy. As designed, the adipose tissue formed from the hydrogel in tumor environment is adjustable according to the request, which exactly replaced the tumor tissue by complete filling the defects caused by tumor atrophy after chemotherapy, resulting in a bright prospect to perfect reconstruct the breast. Moreover, the low pH value around tumor also triggers the AP release from the hydrogel, which could effectively damage bacteria to further promote the adipose regeneration avoiding microbial infections. This shape adjustable hydrogel combining tumor selective chemotherapy, environment triggered antibacterial property as well as tissue regenerative activity would be a promising candidate for breast cancer treatment *via* effective tumor elimination and complete adipose tissue healing, which may be further expanded to the therapy of various cancers.

Declaration of competing interest

The authors declare that they have no known competing financial interests or personal relationships that could have appeared to influence the work reported in this paper.

Acknowledgments

This work was supported by the National High Level Talents Special Support Plan (X.C.), the "Young Talent Support Plan" of Xi'an Jiaotong University (X.C.), the Natural Science Foundation of Shaanxi Province (No. 2022JZ-48 to X.C.), the National Natural Science Foundation of China (No. 82272141 to X.C.) and the Shaanxi Provincial Key Research and Development Plan Project (No. 2023-JC-QN-0260 to X.Q.).

Supplementary materials

Supplementary material associated with this article can be found, in the online version, at doi:10.1016/j.cclet.2023.108343.

References

[1] X. Chen, A.H. Soeriyadi, X. Lu, et al., Adv. Funct. Mater. 24 (2014) 6999–7006.
[2] M.P. Chhaya, F.P.W. Melchels, B.M. Holzapfel, J.G. Baldwin, D.W. Hutmacher, Biomaterials 52 (2015) 551–560.
[3] L.M. Coussens, Z. Werb, Nature 420 (2002) 860–867.
[4] W.T. Dang, T. Li, B. Li, et al., Biomaterials 160 (2018) 92–106.
[5] C.E. DeSantis, J. Ma, A.G. Sauer, L.A. Newman, A. Jemal, CA Cancer J. Clin. 67 (2017) 439–448.
[6] Y.Z. Du, M. Yu, J. Ge, et al., Adv. Funct. Mater. 25 (2015) 5016–5029.
[7] V. Gupta, G.H. Mun, B.N. Choi, et al., Ann. Biomed. Eng. 39 (2011) 2374–2387.
[8] D. Hanahan, R.A. Weinberg, Cell 144 (2011) 646–674.
[9] M.F. Huo, L.Y. Wang, Y. Chen, J.L. Shi, Nat. Commun. 8 (2017) 357.
[10] R.H. Jin, Z.N. Liu, Y.K. Bai, et al., Adv. Funct. Mater. 28 (2018) 1801961.
[11] D.H. Kim, J.T. Martin, D.M. Elliott, L.J. Smith, R.L. Mauck, Acta Biomater. 12 (2015) 21–29.
[12] I.H. Kunkler, L.J. Williams, W.J. Jack, D.A. Cameron, J.M. Dixon, Lancet Oncol. 16 (2015) E105.
[13] Y.X. Chen, B.W. Li, X.H. Chen, et al., Chin. Chem. Lett. 31 (2020) 1153–1158.
[14] G.F. Boafo, Y.J. Shi, Q.Q. Xiao, et al., Chin. Chem. Lett. 33 (2022) 4600–4604.
[15] Z. Ding, X. Pan, X. Wang, H. Xie, Q. Ye, Smart Mater. Med. 2 (2021) 196–208.
[16] G.C. Li, Q. Han, P.J. Lu, et al., Res. China 2020 (2020) 2603048.
[17] X. Qi, F. Jiang, M. Zhou, W. Zhang, X. Jiang, Smart Mater. Med. 2 (2021) 280–291.
[18] X.H. Liu, X.B. Jin, P.X. Ma, Nat. Mater. 10 (2011) 398–406.
[19] Z.N. Liu, X. Chen, X.J. Zhang, J.J. Gooding, Y.S. Zhou, Adv. Healthc. Mater. 5 (2016) 1401–1407.
[20] H.S. Ma, C.A. Jiang, D. Zhai, et al., Adv. Funct. Mater. 26 (2016) 1197–1208.
[21] H.S. Ma, J. Luo, Z. Sun, et al., Biomaterials 111 (2016) 138–148.
[22] T.W.H. Meijer, J.H.A.M. Kaanders, P.N. Span, J. Bussink, Clin. Cancer Res. 18 (2012) 5585–5594.
[23] R. Renneker, M. Cutler, J. Am. Med. Assoc. 148 (1952) 833–838.
[24] J.D. Shao, C.S. Ruan, H.H. Xie, et al., Adv. Sci. 5 (2018) 1700848.
[25] N. Shpaisman, L. Sheihet, J. Bushman, J. Winters, J. Kohn, Biomacromolecules 13 (2012) 2279–2286.
[26] R. Tarzemany, G.Q. Jiang, J.X. Jiang, H. Larjava, L. Hakkinen, Sci. Rep. 7 (2017) 14157.
[27] A.S. Thakor, S.S. Gambhir, CA Cancer J. Clin. 63 (2013) 395–418.
[28] R. Tian, X.Y. Qin, P.Y. Yuan, et al., ACS Appl. Mater. Int. 10 (2018) 17018–17027.
[29] X.C. Wang, T. Li, H.S. Ma, et al., NPG Asia Mater. 9 (2017) e376.
[30] X.C. Wang, F. Lv, T. Li, et al., ACS Nano 11 (2017) 11337–11349.
[31] X.C. Wang, B. Ma, J.M. Xue, et al., Nano Lett. 19 (2019) 2138–2147.
[32] Y.W. Xi, J. Ge, Y. Guo, B. Lei, P.X. Ma, ACS Nano 12 (2018) 10772–10784.
[33] B.W. Yang, J.H. Yin, Y. Chen, et al., Adv. Mater. 30 (2018) 1705611.
[34] Y.C. Chu, T. Sun, C. Jiang, Chin. Chem. Lett. 33 (2022) 4157–4168.
[35] Y. Yang, L.Y. Chu, S.B. Yang, et al., Acta Biomater. 79 (2018) 265–275.
[36] Q. Zhan, B.Y. Shen, X.X. Deng, et al., Int. J. Nanomed. 8 (2013) 2465–2472.
[37] N.S. Qiu, X.R. Liu, Y. Zhong, et al., Adv. Mater. 28 (2016) 10613–10622.
[38] X. Chen, Z.N. Liu, S.G. Parker, et al., ACS Appl. Mater. Int. 8 (2016) 15857–15863.
[39] M. Zasloff, Nature 415 (2002) 389–395.
[40] N. Pante, M. Kann, Mol. Biol. Cell. 13 (2002) 425–434.